Optical and Quantum Electronics (2024) 56:1384
https://doi.org/10.1007/s11082-024-07318-2

DFT study of structural, elastic and optoelectronic characteristics of novel Rb_2CaSnX_6 (X = Cl, I) double halide perovskites for optoelectronic applications

Shaukat Ali Khattak[1] · Saikh Mohammad Wabaidur[2] · Asma A. Alothman[2] · Mudasser Husain[3] · Malak Azmat Ali[4] · Nasir Rahman[5] · Irfan Ullah[1] · Syed Zulfiqar[1] · Gul Rooh[1] · Tahirzeb Khan[1] · Gulzar Khan[1]

Received: 23 March 2024 / Accepted: 28 July 2024 / Published online: 6 August 2024

Abstract
We evaluate the structural, optoelectronic, and mechanical characteristics of the novel $Rb_2CaSnCl_6$ and Rb_2CaSnI_6 through density functional theory within the WIEN2K framework. The formation energies and volume optimization provide evidence for the structural stability of these compounds. The optimized lattice constants for $Rb_2CaSnCl_6$ and Rb_2CaSnI_6 are found to be 11.21 Å and 12.45 Å, respectively while their respective formation energies are calculated as − 2.5 Ry and − 1.6 Ry. Similarly, the grounds state energies are calculated − 31,184.32 Ry and − 111,074.60 Ry. We find that $Rb_2CaSnCl_6$ is an insulator with a bandgap energy of 3.50 eV when the modified Becke-Johnson (mBJ) approximation is applied and that Rb_2CaSnI_6 is directly semiconducting with a wide bandgap energy of 2.70 eV. Evaluations of mechanical stability show that both materials are mechanically stable and their constituent atoms are bound together by ionic interactions, indicated by the positive value of Cauchy's pressure: 46. 32 and 21.93 for $Rb_2CaSnCl_6$ and Rb_2CaSnI_6, respectivley. Nevertheless, our investigation showed that Rb_2CaSnI_6 behaves as a ductile material while $Rb_2CaSnCl_6$ is brittle. We also investigate a variety of optical characteristics such as dielectric function, refraction, reflectivity, energy loss function, and extinction coefficient. The static dielectric function was found to be 2.9 and 4.3 for $Rb_2CaSnCl_6$ and Rb_2CaSnI_6, respectively. Rb_2CaSnI_6 exhibited greater optical conductivity, indicative of it being a better metallic than the $Rb_2CaSnCl_6$. The optical investigation suggests that these materials have a great deal of promise for cutting-edge optoelectronic applications, especially in the ultraviolet (UV) spectrum due to their large electronic band gap. These results offer a solid basis for future research into these intriguing materials by experimentalists.

Keywords WIEN2K · DFT · Double halide perovskites · Structural properties · Electronic properties · Optical properties · Mechanical properties

Extended author information available on the last page of the article

1 Introduction

It has been longed for decades to obtain novel compounds with diverse characteristics which have driven intensified quest for such materials and manifested in the present cutting-edge progress in the technology. Among these compounds (Khattak et al. 2022a; Saddique et al. 2022), the halide perovskites (Khattak et al. 2022b) have been considered distinctive due to their potential use in multiple fields such as optoelectronics (Paul et al. 2023), photovoltaics (Jena et al. 2019) and solid-state lighting (Adjokatse et al. 2017). This has been followed by the shifting attention to their double form, i.e., double halide perovoksites (Muscarella and Hutter 2022; Ali et al. 2023a, b; Husain et al. 2023; Rahman et al. 2023), as double halide perovskites offer a better alternative: their properties can be tailored by altering their composition. Double halide perovskites drew a massive interest to be studied as they are adaptable extraordinarily and demonstrate promising electrical, structural, mechanical and structural characteristics (Muscarella and Hutter 2022; Ju et al. 2018). The double halide perovskites based on lead have been found useful for applications in solar cell devices (Rosales et al. 2017). However, since the lead is toxic, such perovskites can't be fully exploited (Ren et al. 2022). Therefore, this has triggered the investigation of lead-free double perovskites which have the same advantages offered by the double perovskites and are free from the downsides posed by the lead-based double halide perovskites (Gao et al. 2021).

Lead-free double perovskites with the formula $A_2B^IB^{III}X_6$ have garnered attention for their potential in diverse sustainable and renewable energy applications (Saeed et al. 2022; Alnujaim et al. 2022; Islam et al. 2021). Here A represents a cation belonging to the s/p block; B^I and B^{III} also denote cations but form the p/d/f section while an anion is represented by X, typically halides or oxides ions (Mir and Gupta 2021; Thawarkar et al. 2021). Such compounds have been proved useful because they have wonderful physical characteristics: they are modifiable and have appropriate band gap energies and low effective charge carrier masses, high optical absorption coefficients, extensive diffusion lengths, strong defect tolerance, and adaptable compositional flexibility (Grätzel 2014; Barrows et al. 2014; Xing et al. 2013). These compounds offer a vast array of potential combinations, each with a wide spectrum of optoelectronic and thermoelectric characteristics. Over the recent years, double perovskites have been extensively explored for applications in photoluminescence, photovoltaics, and thermoelectric (Soni et al. 2022; Bhorde et al. 2021; Tang and Tang 2023). Notably, double perovskites containing tin (Sn) have demonstrated excellent properties. Landini et al. (2022) investigated $Cs_2GeSnCl_6$ and $Cs_2GeSnBr_6$ in a double perovskite structure with a space group of Fm3m, determining band gaps of 1.35 eV and 0.85 eV, respectively. Spectroscopic limited maximum efficiency calculations indicated values of 27% and 21% for $Cs_2GeSnCl_6$ and $Cs_2GeSnBr_6$ respectively, positioning them as effective absorbers for solar cells. Mukaddar and Saurabh (Sk and Ghosh 2022) employed the DFT approach to report on the structural, optoelectronic, and photovoltaic properties of $Cs_2GeSnCl_6$, revealing a direct band gap of 0.91 eV and a power conversion efficiency of 16.35%. The structural, mechanical, optical, and thermoelectric properties of Cs_2GeSnX_6 (X = Cl, Br) have been investigated, suggesting their suitability for optoelectronic and thermoelectric applications (Behera and Kumar Mukherjee 2023). These findings underscore the potential of Sn-based double perovskites as alternatives to lead-based perovskites. However, the quest for a better alternative to that is still underway. In this regard, Rb_2CaSnX_6 (X = Cl, I) remains unexplored within this category where the alkali atom such as Rb offers stability through charge transfer like in fullerene intercalated compounds (Poloni et al. 2008a, b). This study, employing density functional theory (DFT),

addresses this gap by systematically investigating the structural, electronic, and optical properties of these compounds. We explored the electronic characteristics of Rb_2CaSnX_6 (X = Cl, I) in detail, analyzing their electronic band structures, using state-of-the-art Density Functional Theory (DFT) computations. We carefully investigate the bandgap, which is a crucial characteristic defining its optoelectronic value. We also widen our focus to include these materials' mechanical characteristics: how they react to outside pressures and situations using simulation approaches, with a focus on characteristics like ductility, hardness, and flexibility. This research not only fills a theoretical void in the scientific literature but also serves as a reference for future studies on Rb_2CaSnX_6 (X = Cl, I) double perovskite compounds. The results highlight the feasibility of utilizing Rb_2CaSnX_6 (X = Cl, I) compounds in electronic devices.

2 Materials and methods

The studied compounds were subjected to computational analysis using the WIEN2K code. We applied the FP-LAPW method, as described by Blaha and his coworkers (Blaha et al. 1990). Notably, our calculations did not consider the effects of spin–orbit coupling (SOC), following the approach outlined by Vijayakumar and Gopinathan (1996).

For structural optimization, we employed the GGA method, initially introduced by Kohn and Sham (1965). This method has been coded in the WIEN2K, one of the DFT simulation codes, as documented by Blaha et al. (2019). To attain the structural optimization of the materials in terms of geometry and conduct calculations related to mechanical and optoelectronic characteristics, we utilized a Monkhorst–Pack sampling scheme. Specifically, a k-point sampling grid with dimensions of $10 \times 10 \times 10$ was employed to adequately sample the Brillouin zone (BZ).

Throughout the structural optimization process, we adjusted both ionic coordinates and lattice volumes to ensure that residual forces remained below 0.01 eV.

A convergence criterion of 10^{-4} eV was established for self-consistent calculations related to energy.

In the analysis of optical and electronic properties, we employed the Tran Blaha modified Becke Johnson (TB-mBJ) potentials as introduced by Koller et al. (2012) To distinguish between core and valence states, a cutoff energy of -6.0 Ry was determined. Additionally, we chose the parameters $RMT \times K_{max} = 7.0$. We established the 0.001-Ry convergence criterion, i.e., the convergence was obtained by becoming the total energy of the system constant, following the self-consistent calculations. The optical properties were determined by utilizing the OPTIC package integrated into Wien2k where the "Joint density of states" method has been employed, which was adapted with the inclusion of the pertinent dipole matrix elements as specified in the provided references (Ambrosch-Draxl et al. 1995; Abt et al. 1994; Ambrosch-Draxl and Sofo 2006). The elastic properties were determined by exploiting the IRelast package, interfaced with the Wien2K (Jamal et al. 2018). We characterized the optical characteristics of the compounds by calculating the complex dielectric function $[\varepsilon(\omega)]$ as given by Eq. (1).

$$\varepsilon(\omega) = \varepsilon_1(\omega) + \varepsilon_2(\omega), \tag{1}$$

where $\varepsilon_1(\omega)$ and $\varepsilon_2(\omega)$ represent photon dispersion and energy absorption capacity, respectively. The $\varepsilon_2(\omega)$ is given by Eq. 2:

$$\varepsilon_2(\omega) = \frac{2\pi e^2}{\Omega\varepsilon_o} \sum_{c,v} \sum_{k} \left|\psi_k^c\right| ur \left|\psi_k^v\right|^2 \delta\left(E_k^c - E_k^v - h\omega\right), \tag{2}$$

where, k is the direction of polarization of the E field with a full isotropic type of average value in the polycrystalline materials, Ω represents the unit cell volume, ω denotes frequency of incident light while c, v, denote the conduction and valence bands, respectively.

The $\varepsilon_1(\omega)$ and $\varepsilon_2(\omega)$ were used to calculate the energy loss function $[L(\omega)]$, given by Eq. (3).

$$L(\omega) = \frac{\varepsilon_2(\omega)}{\varepsilon_1^2(\omega) + \varepsilon_2(\omega)(\omega)}. \tag{3}$$

The absorption coefficient $[I(\omega)]$ was computed using Eq. (4):

$$I(\omega) = \frac{\sqrt{2}\omega}{c}\left(\sqrt{\varepsilon_1^2(\omega) + \varepsilon_2^2(\omega)} - \varepsilon_1(\omega)\right)^{\frac{1}{2}}. \tag{4}$$

Equation (5) was used to calculate the reflectivity,

$$R(\omega) = \left|\frac{\sqrt{\varepsilon_1(\omega) + i\varepsilon_2(\omega)} - 1}{\sqrt{\varepsilon_1(\omega) + i\varepsilon_2(\omega)} + 1}\right|^2. \tag{5}$$

The refractive indices $n(\omega)$ was determined by Eq. (6),

$$n(\omega) = \left(\frac{1}{2}\left[\sqrt{\varepsilon_1^2(\omega) + \varepsilon_2^2(\omega)} + \varepsilon_1(\omega)\right]\right)^{\frac{1}{2}}. \tag{6}$$

Equation (7) was employed to compute the extinction coefficient $k(\omega)$,

$$k(\omega) = \left(\frac{1}{2}\left[\sqrt{\varepsilon_1^2(\omega) + \varepsilon_2^2(\omega)} - \varepsilon_1(\omega)\right]\right)^{\frac{1}{2}}. \tag{7}$$

The real optical conductivity $\sigma^{real}(\omega)$ was found while using Eq. (8),

$$\sigma^{\text{real}}(\omega) = \varepsilon_0(\omega)\varepsilon_1(\omega), \tag{8}$$

where $\varepsilon_0(\omega)$ is the static dielectric function.

3 Results and discussions

3.1 Structural and mechanical properties

The selected halide-perovskites, Rb_2CaSnX_6 (X = Cl, I), have a cubic structure with the Fm-3 m (No. 225) space group. The structure of the studied materials is given in Fig. 1.

The fractional coordinates of the Rb, Ca, Sn and X atoms (X = Cl, I) are (0.25, 0.25, 0.25), (0, 0, 0), (0.5, 0.5, 0.5), and (0.25, 0, 0), respectively, and they correspond to the 8c, 4a, 4b, and 24e Wyckoff locations. Figure 1 illustrates the 40 atoms in the unit cell of the double perovskite halides $Rb_2CaSnX6$ (X = Cl, I) with four formula units. The ground

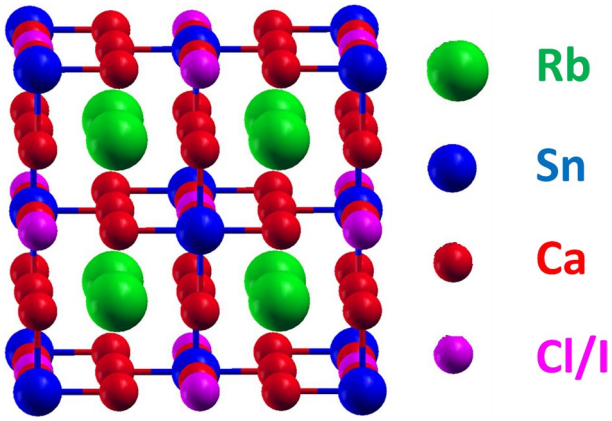

Fig. 1 Cubic structure for alkali metal-based double halide perovskites: $Rb_2CaSnCl_6$/Rb_2CaSnI_6

state energy of all three composites is negative; E_o characterizes the structural stability of Rb_2CaSnX_6 (where X = Cl, I).

Structural optimization or geometry optimization was performed to compute the ground-state energy. For this purpose, the energy-volume curve is fitted with the Birch-Murnaghan equation of state (EOS), which provides the structural properties (Tyuterev and Vast 2006) of the compounds such as bulk modulus (B_0) and the derivative of the bulk modulus, ground state volume and lattice parameter (a_0). Figure 2 displays the fitted Birch-Murnaghan equation of states to the data of the energy-volume curve.

The structural parameters obtained by fitting the Birch Murnaghan state of the equation to the data are listed in Table 1, which have also been compared with those of other similar previously-reported compounds. Due to the rising ionic radii of the X-anion from Cl to I, the a_0 increases from 11.21 Å to 12.45 Å for $Rb_2CaSnCl_6$ to Rb_2CaSnI_6. The formation energies of the compounds were computed through the Eq. (9) given in the work of Khattak et al. (2023):

$$H_f = E_{Rb_2CaSnX_6} - \left(aE_{Rb} + bE_{Ca} + cE_{Sn} + dE_X\right), \tag{9}$$

where $E_{Rb_2CaSnX_6}$ is the total energy of the compound, a, b, c and d shows the number of individual atoms. $E_{Rb}, E_{Ca}, E_{Sn} and E_X$ represent the energy of Rb, Ca, Sn and X (Cl, I). The negative formation energy of the compounds indicates their stability.

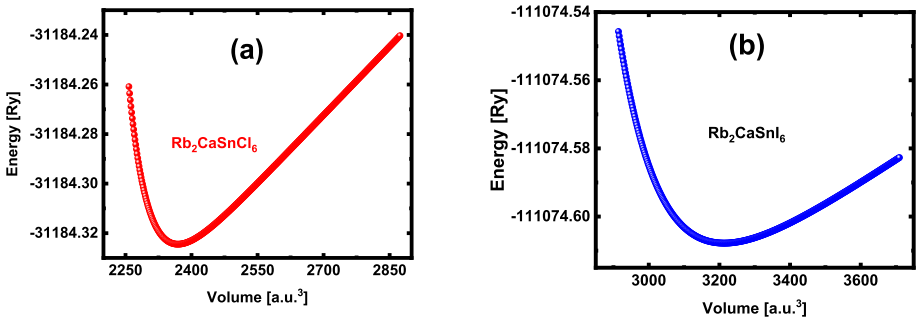

Fig. 2 Volume-optimization curves for the cubic structure of alkali metal-based halide double perovskite s: **a** $Rb_2CaSnCl_6$ and **b** Rb_2CaSnI_6, obtained by exploiting the GGA-PBE potential

Table 1 The structural parameters of the cubic structure of alkali metal-based halide double perovskites, i.e., $Rb_2CaSnCl_6$ and Rb_2CaSnI_6: i.e., lattice constant (a_0), optimized volume (V_0), Bulk modulus (B_0), pressure derivative (B'), ground-state energy (E_0) and formation energy (H_f)

Compound	Structural parameters						References
	a_0 (Å)	V_0 (a.u^3)	B_0 (GPa)	B'	E_0 (Ry)	H_f (Ry)	
Rb_2GeSnI_6	12.22	1823.07	16.86	5.0	0.49	− 2.60	43
Cs_2GeSnI_6	12.28	1851.24	16.59	5.0	0.57	− 1.84	43
$K_2AgAsCl_6$	10.41	–	31.47	–	–	− 3.10	44
$K_2AgAsBr_6$	10.96	–	25.92	–	–	− 2.50	44
$Rb_2CaSnCl_6$	11.21	2381.27	69.52	13.6382	− 31,184.32	− 2.5	Present work
Rb_2CaSnI_6	12.45	3262.45	23.78	11.4139	− 111,074.60	− 1.6	Present work

The parameters have also been compared with those of other similar previously-reported compounds

The determination of thermodynamic stability often relies on the computation of Gibbs free energy (G). In this study, the calculated values for G using the Gibbs2 computational code (Blanco et al. 2004) were determined to be -3.28×10^7 kJ/mol for $Rb_2CaSnCl_6$ and -5.63×10^7 kJ/mol for Rb_2CaSnI_6. The negative values obtained affirm the thermodynamic stability of both double perovskite compounds. In thermodynamics, a negative Gibbs free energy indicates the spontaneous and energetically favorable nature of a reaction under specific conditions. Consequently, the negative G values for $Rb_2CaSnCl_6$ and Rb_2CaSnI_6 suggest their thermodynamic stability under the given computational parameters.

The determination of elastic constants is crucial to investigating a material's elastic properties since it shows how the material responds to outside forces and sheds light on its mechanical properties. These constants establish whether the material is mechanically stable and tough or not. The energy is applied in accordance with the lattice strain for maintaining the volume constants(State and Physics: Ashcroft, Neil W., Mermin, N. 2022). The IRelast package was exploited for the computation of the elastic constants (Jamal et al. 2018). C_{11}, C_{12} and C_{44} are the elastic constants (C_{ij}) in the case of a cubic structure. Equations detailed in the work of Khattak et al. (2022a) were used to find these parameters. With the halogen atom switching from Cl to I, a decrease in the bulk, shear and Young's moduli of Rb_2CaSnX_6 (X = Cl, I) was noted. The Born-Huang stability condition is used to examine the materials in the cubic phase whether they are mechanically stable or not (Karki et al. 1997; Mouhat and Coudert 2014):

$$C_{11}-C_{12}>0;C_{11}>0;C_{44}>0;C_{11}+2C_{12}>0$$

Both materials meet the Born-Huang stability criterion and all the stability standard results, confirming that the Rb_2CaSnX_6 (X = Cl, I) compounds are mechanically stable. The values of C_{12}–C_{44}, or Cauchy's pressures, can be used to calculate the nature of chemical bonding between atoms. The positive values of Cauchy's pressure for both materials in Table 1 suggest the ionic bonds among the atoms. To determine if the materials under consideration are brittle or ductile, we computed the Poisson's. A material is classified as brittle if its Poisson's ratio value is less than 0.26 GPa; otherwise, it is ductile. Similarly, a material is brittle if the computed Pugh ratio is less than 1.75 GPa; otherwise, it is ductile. Table 2's estimated Poisson's and Pugh ratio values indicate that $Rb_2CaSnCl_6$ is brittle while ductility is exhibited by Rb_2CaSnI_6.

Table 2 Elastic parameters for $Rb_2CaSnCl_6$ *to* Rb_2CaSnI_6: elastic stiffness coefficients (C_{11}, C_{12} and C_{44}), bulk modulus (B) and Zener's constant (A)

Elastic parameters	$Rb_2CaSnCl_6$	Rb_2CaSnI_6
C_{11}(GPa)	51.33	30.66
C_{12}(GPa)	5.01	8.73
C_{44}(GPa)	3.42	0.80
B (GPa)	20.20	16.09
A	0.1	0.1
G_v(GPa)	48.4	22.4
G_R(GPa)	4.9	1.0
G(GPa)	26.6	11.7
E(GPa)	55.7	28.3
V	0.1	0.3
B/G	0.75	1.37

G_v, G_R and G are Voigt shear modulus, Reuss shear modulus, and mean of G_v and G_R, respectively. E is the Elastic modulus, V is the Poisson's ratio, and B/G is the Pugh ratio of bulk to shear moduli

3.2 Electronic properties

A material's band structure shows the permitted bands or energy levels that electrons can occupy, which is illustrated by a graph of energy vs. momentum. The energy dispersion and permitted electronic states in the material are revealed by the band structure. A material's electrical, optical, and thermal properties are largely determined by its band structure. The electronic energy states distribution in a compound is described by the density of states (DOS). It shows how many different energy states are possible for each unit's volume and energy range. The distribution and population of electrons at various energy levels are revealed by the DOS, which helps grasp the electronic transport, optical absorption, and thermal characteristics of compounds. Using the optimized lattice constants, computational research was done on the compounds' electronic characteristics.

Figure 3 depicts the band structures that were properly analyzed to study the electronic characteristics of Rb_2CaSnX_6 (X = Cl, I). For $Rb_2CaSnCl_6$ and Rb_2CaSnI_6, the calculations revealed that they are direct-bandgap semiconductors with bandgap energies of 3.50 eV, and 2.70 eV, respectively. An increased lattice parameter causes a decrease in the ion–electron coulomb interaction of X-anions (X = Cl, I) from $Rb_2CaSnCl_6$ to Rb_2CaSnI_6, which in turn results in a decreased band gap while moving from $Rb_2CaSnCl_6$ to Rb_2CaSnI_6. The Coulomb interaction in the chlorine anion is greater than that in the iodine ion as the ionic radius of Cl is smaller than that of the I. The weaker ion–electron interaction in the I than in the Cl results in a decreased electronic bandgap for the Rb_2CaSnI_6.

Table 3 lists the calculated bandgap values of the present compounds with those of similar double perovskites, previously reported.

These results have several noticeable implications in various fields both scientifically and technologically: To design and develop new materials with tailorable properties, it is imperative to grasp their structural and elastic properties. The calculated structural and mechanical properties such as lattice constants, bulk modulus, and elastic constants can help in synthesizing and engineering the material for a particular purpose. The mechanical strength exhibited by their ductility and mechanical stability suggests that they can be used where toughness and flexibility are required. The revealed direct bandgap of these

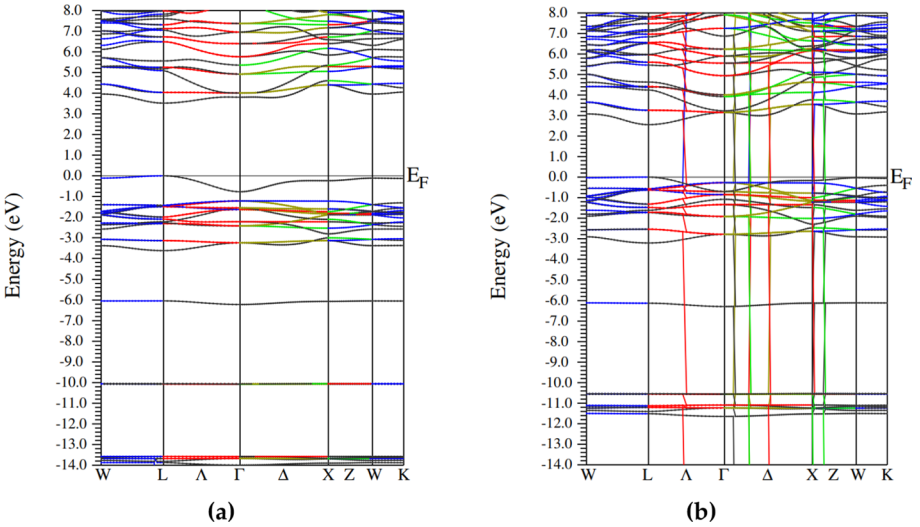

Fig. 3 Band structure for the cubic alkali metal-based halide double perovskites: **a** $Rb_2CaSnCl_6$ and **b** Rb_2CaSnI_6, obtained by exploiting the modified Becke-Johnson (mBJ) method

Table 3 Comparison of calculated bandgap values of $Rb_2CaSnCl_6$ and Rb_2CaSnI_6 with those of similar double perovskites previously reported

Compound	Calculated bandgap (eV) in this study	Reported bandgap (eV) in previous studies
$Rb_2CaSnCl_6$	3.50	Present work
$Cs_2CaSnCl_6$	3.58	49
Rb_2CaSnI_6	2.70	Present work
Cs_2CaSnI_6	2.60	49
Rb_2GeSnI_6	0.49 eV	43

semiconductors indicates that these materials can be used as active materials in optoelectronic devices. Particularly, the Rb_2CaSnI_6 with the decreased band gap is promising for optoelectronic devices having more efficiency. Furthermore, the suitability of the materials for conversion technology and energy storage is decided by their bandgap. The calculated bandgap energies suggest their applications in energy devices such as memory devices because less energy is required for set and rest, making the memory storage devices more efficient.

3.3 Optical properties

When a material interacts with light, its optical properties include how it absorbs, reflects, transmits, and emits electromagnetic radiation in the visible, ultraviolet, and infrared regions. These characteristics are crucial for several applications in photonics, materials science, optoelectronics, and other related fields. A material's electronic band structure largely determines its optical properties50.

The two compounds' optical characteristics were examined, considering incident photon energies as high as 14 eV. The dielectric function $\varepsilon(\omega)$ spectrum for both materials

are shown in Fig. 4, which offers information about how the material reacts to incident photons at different energies. As the losses are related to polarization effects, the material's capacity to store electric energy is represented by $\varepsilon_1(\omega)$ in Fig. 4(a). The dielectric function's static frequency component, denoted by $\varepsilon_1(0)$, is 2.9 and 4.3 for $Rb_2CaSnCl_6$ and Rb_2CaSnI_6, respectively, in the zero-frequency range, which is consistent with the bandgap values shown in Fig. 3, i.e, for the compounds with increased bandgap value ($Rb_2CaSnCl_6$), the static dielectric function is lower than that for the compound with decreased bandgap (Rb_2CaSnI_6). For $Rb_2CaSnCl_6$ and Rb_2CaSnI_6, the real component's maximum values, ε_1, in the complex dielectric function are 5.1 at 3.74 (UV range) and 7.7 at 2.8 eV (visible range), respectively. The higher dielectric constant for Rb_2CaSnI_6 than for the $Rb_2CaSnCl_6$ can be attributed to multiple factors: (1) upon exposure to the external electric field in electromagnetic radiation, the electrons in Rb_2CaSnI_6 get more displaced than in the $Rb_2CaSnCl_6$, hence more electronic polarization effect takes place in the former than the latter; (2) more atomic polarizability (distortion of electron clouds around the atoms) occurs in Rb_2CaSnI_6 than in the $Rb_2CaSnCl_6$. It is evident from the $\varepsilon_1(\omega)$ spectrum that the curve takes on negative values at higher energies, meaning that these materials reflect electromagnetic waves in this range of frequencies. The maximum value of 5. 1 $\varepsilon_1(\omega)$ for $Rb_2CaSnCl_6$ indicates that the material has good dielectric characteristics in the UV range. This implies that the material is promising for applications where UV light responsiveness is required: like photodetectors and UV sensors. On the other hand, Rb_2CaSnI_6 with 7.7 as the maximum $\varepsilon_1(\omega)$ value at 2.8 eV, i.e., in the visible range, suggests that it is suitable for photovoltaic cells and LEDs, the devices working within the visible spectrum. Additionally, Fig. 4(b) shows how the imaginary component $\varepsilon_2(\omega)$ of the dielectric function behaves, representing how these compounds absorb incident radiation. The energy range of roughly 3–9 eV is where the dominant peaks in the spectrum are found. Notably, the imaginary component spectra in both materials show zero values up until the point at which absorption begins, which is the band gap energy corresponding to the photon energy, i.e., optical bandgap, which is nearly equal to their electronic bandgap shown in Fig. 3. For the optical transitions between the valence band maxima (VBM) and the conduction band minima (CBM), this is the transition point.

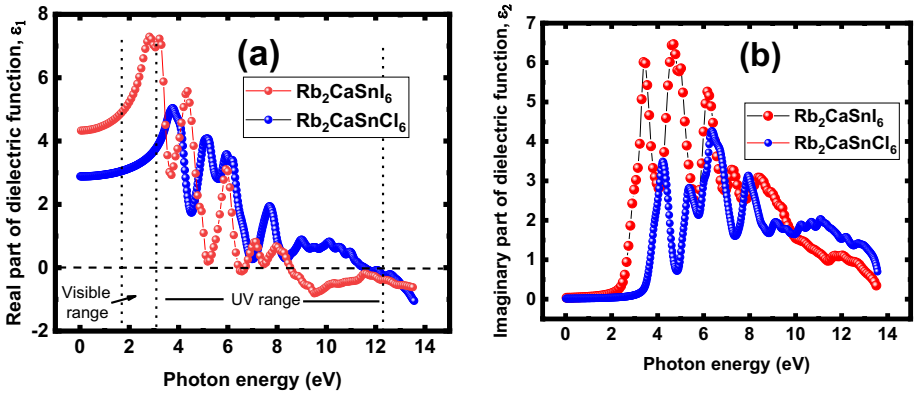

Fig. 4 **a** Real and **b** imaginary parts of dielectric function for the cubic alkali metal-based halide double perovskites, i.e., $Rb_2CaSnCl_6$ and Rb_2CaSnI_6, represented by blue and red data points, respectively

A material's ability to link the induced current density and the induced electric field strength at different frequencies is known as optical conductivity. The optical conductivity σ(ω), both its real and imaginary parts, of the two compounds are shown in Fig. 5. Both materials' optical conductivity spectra show a comparable pattern. The spectra in Fig. 5(a) clearly show that the optical conductivity is zero until the incident photon energy crosses the band gap energy. For $Rb_2CaSnCl_6$ and Rb_2CaSnI_6, the maximum peak of the real part of optical conductivity σ(ω) is observed to be 3.2×10^{15}/sec and 4.0×10^{15}/sec, respectively, i.e., with greater optical conductivity, the Rb_2CaSnI_6 demonstrates lesser insulation (or greater metallicity) than the $Rb_2CaSnCl_6$, which is consistent with the band structure profiles of both compounds given in Fig. 3. Similarly, the imaginary part of the optical conductivity is given in Fig. 5(b), where it is in the negative values up to around 11.63 eV and 6.57 eV for $Rb_2CaSnCl_6$ and Rb_2CaSnI_6, respectively. This suggests that rather than absorbing the incident light, both materials behave as a gain medium at the corresponding frequencies of these energy ranges, i.e., they can amplify the light through stimulated emission and are promising for laser and optical amplification.

The refractive index is a dimensionless measurement that expresses how well an optical medium bends light. It has a linear dependence on wavelength because of interactions between various wavelengths and the medium's atoms. The refractive index n(ω) and spectra of the extinction coefficient, κ(ω), for $Rb_2CaSnCl_6$ and Rb_2CaSnI_6, are shown in Fig. 6(a) and (b), respectively. The refractive index at zero-incident photon energy is represented by the static refractive index, or n (0). The values of n (0) for $Rb_2CaSnCl_6$ and Rb_2CaSnI_6 are 1.7 and 2.1, respectively. For both materials, the n(ω) spectra show similar behavior: a steep decline that becomes negative at 11.36 eV and 9.26 eV for $Rb_2CaSnCl_6$ and Rb_2CaSnI_6, respectively. The negative refractive index beyond these energies shows these compounds exhibit negative refraction, i.e., the light starts traveling in the opposite direction to that observed commonly in the materials.

The extinction coefficient describes how much light is absorbed by a substance at a given color and frequency and how much of the light's intensity is lost as it travels through the substance. It gives details on how deeply a material can absorb light with a particular wavelength. Low extinction coefficient materials tend to transmit light, giving the impression that they are transparent, especially at certain wavelengths. Both the material and the incident light's

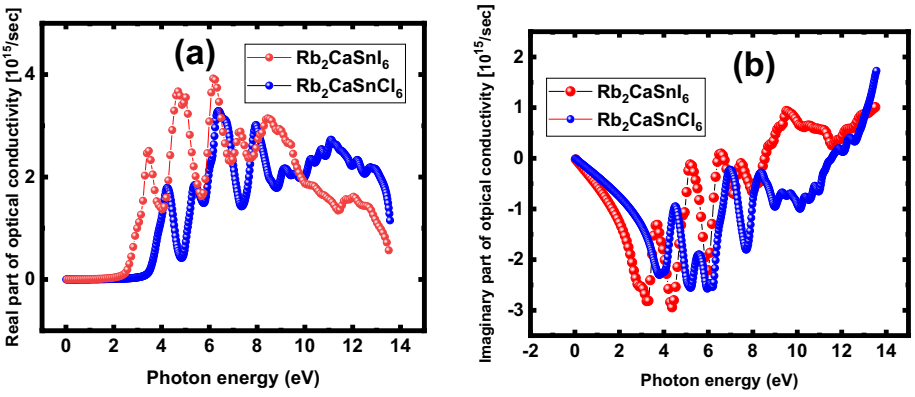

Fig. 5 **a** Real and **b** imaginary parts of optical conductivity for the cubic alkali metal-based halide double perovskites, i.e., $Rb_2CaSnCl_6$ and Rb_2CaSnI_6, represented by blue and red data points, respectively

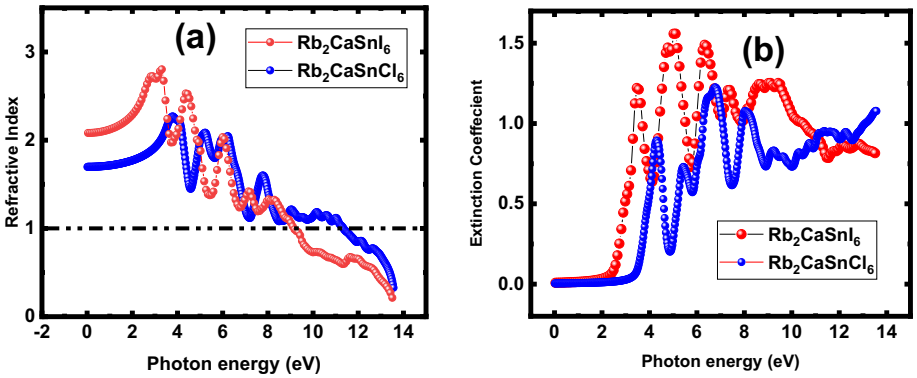

Fig. 6 **a** Refractive index and **b** extinction coefficient for the cubic alkali metal-based halide double perovskites, i.e., $Rb_2CaSnCl_6$ and Rb_2CaSnI_6, represented by blue and red data points, respectively

wavelength have an impact on the extinction coefficient. Light with energies below the band gap cannot induce electron transitions from the VB to the CB in semiconductor materials, which have high extinction coefficients. As a result, it's possible that light won't be absorbed.

The probability of photon absorption is determined by the possibility of photon-electron interaction during the electron's energy band transition. By interacting with photons, only electrons at the valence band's immediate edge can effectively absorb them. As a result, absorption is minimal if the photon's energy closely resembles the band gap value. On the other hand, electrons with energies farther from the band gap can interact with photons as photon energy increases. Increased photon absorption results from a greater number of electrons interacting with the photon due to the wider range of electron energies. The absorption coefficients displayed by various materials have an impact on the materials chosen for solar cell design51.

The extinction coefficient in Figure (b) shows that over the energy range of 0–14 eV, the Rb_2CaSnI_6 demonstrates a higher extinction coefficient than the $Rb_2CaSnCl_6$.

Reflectivity is represented by Fig. 7(a) where the reflectivity R(ω) spectral curves for Rb_2CaSnX_6 (X = Cl, I) perovskites are displayed. $Rb_2CaSnCl_6$ and Rb_2CaSnI_6 have static reflectivity values of R(ω) of 0.06 and 0.001, respectively. There is no significant increase in the reflectivity until 12 eV and 9 eV for $Rb_2CaSnCl_6$ and Rb_2CaSnI_6, respectively. However, the R(ω) spectra for both compounds show an upward trend with increasing photon energy, afterward. In general, the Rb_2CaSnI_6 is more reflective than the $Rb_2CaSnCl_6$. Figure 7(b) shows the energy loss functions versus photon energy in the energy range of 0–14 eV. The energy loss function for both materials slightly fluctuates between 0 and 6 eV and for the higher energies than the 6 eV, there is a noticeable increase in it: the Rb_2CaSnI_6 exhibits a higher energy loss function than the $Rb_2CaSnCl_6$. This suggests that Rb_2CaSnI_6 dissipates more energy than $Rb_2CaSnCl_6$ during its interaction with electromagnetic radiation.

4 Conclusion

First-principles calculations within the WIEN2K framework were used to determine the structural, optoelectronic, and mechanical properties of the compounds under investigation. The optimized lattice constants for $Rb_2CaSnCl_6$ and Rb_2CaSnI_6 were determined

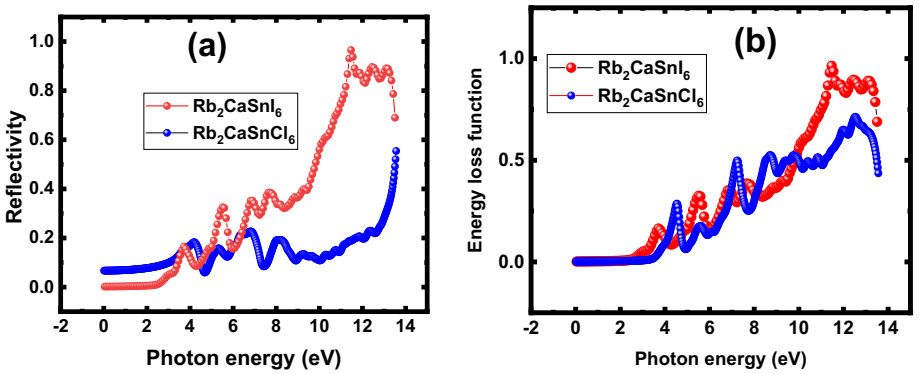

Fig. 7 **a** Reflectivity and **b** energy loss function for the alkali metal-based double perovskites halide, i.e., $Rb_2CaSnCl_6$ and Rb_2CaSnI_6, represented by blue and red data points, respectively

to be 11.21 Å and 12.45 Å, respectively while their respective formation energies were found as − 2.5 Ry and − 1.6 Ry. Volume optimization and the negative value of formation energy supported the structural stability of both compounds. By using the mBJ approximation, the $Rb_2CaSnCl_6$ was found to be an insulator with a bandgap energy of 3.50 eV while Rb_2CaSnI_6 exhibited a direct semiconducting nature with a wide bandgap energy of 2.70 eV. It was also shown that both materials are mechanically stable, and the constituent atoms are bonded with each other by ionic bonds, indicated by the positive value of Cauchy's pressure: 46. 32 and 21.93 for $Rb_2CaSnCl_6$ and Rb_2CaSnI_6, respectivley. The $Rb_2CaSnCl_6$ exhibited brittleness while the ductile nature of the Rb_2CaSnI_6 was revealed. The static dielectric function was found to be 2.9 and 4.3 for $Rb_2CaSnCl_6$ and Rb_2CaSnI_6, respectively. Rb_2CaSnI_6 exhibited greater optical conductivity, indicative of it being a better metallic than the $Rb_2CaSnCl_6$. The examination of different optical properties showed that these materials have a significant potential for advanced optoelectronic applications, especially in the ultraviolet (UV) region, especially given their wide electronic band gap. Experimentalists now have the chance to investigate these materials more thoroughly thanks to these findings.

Acknowledgements The authors would like to thank the Researchers Supporting Project Number (RSP2024R448), King Saud University, Riyadh, Saudi Arabia. The authors would like to thank the National Research Program for Universities (NRPU), Higher Education Commission Pakistan, No. 20-15131/NRPU/R&D/HEC/2021. The authors would like to thank National Research Program for Universities (NRPU), Higher Education Commission Pakistan, No. 20-15128/NRPU/R&D/ HEC/2021.

Author contributions Shaukat Ali Khattak: software, data curation: conceptualization, project administration, writing—original draft. Saikh Mohammad Wabaidur: data curation, Asma A. Alothman: software, data curation. Mudasser Husain: conceptualization, project administration. Malak Azmat Ali: conceptualization, project administration. Nasir Rahman: conceptualization, project administration. Irfan Ullah: conceptualization, project administration. Syed Zulfiqar: data curation. Gul Rooh: software, data curation. Tahirzeb Khan: software, data curation. Gulzar Khan: project administration.

Data Availability No datasets were generated or analysed during the current study.

Declarations

Conflict of interest The authors declares that they have no conflict of interest.

References

Abt, R., Ambrosch-Draxl, C., Knoll, P.: Optical response of high temperature superconductors by full potential LAPW band structure calculations. Phys. B Condens. Matter. **194–196**, 1451–1452 (1994). https://doi.org/10.1016/0921-4526(94)91225-4

Adjokatse, S., Fang, H.H., Loi, M.A.: Broadly tunable metal halide perovskites for solid-state light-emission applications. Mater. Today **20**(8), 413–424 (2017). https://doi.org/10.1016/J.MATTOD.2017.03.021

Ali, A., Khan, S.M., Khan, G., Gul, B., Tawfeek, M.A., Azam, S., Abbas, F., Zulfiqar, S., Khattak, S.A., Khan, T., Shah, S.K.: The spin-polarized electronic and optical properties of novel Ba_2TaXO_6 (X = Co, Fe, In) for optoelectronic applications: an ab-initio study. J. Solid State Chem. **326**, 124211 (2023). https://doi.org/10.1016/J.JSSC.2023.124211

Ali, M.A., Musa Saad, M., Tighezza, A.M., Khattak, S., Al-Qaisi, S., Faizan, M.: First-principles calculations of novel lead-free X_2GeSnI_6 (X = Rb, Cs) double perovskite compounds for optoelectronic and energy exploitations. J. Inorg. Organomet. Polym. Mater. (2023). https://doi.org/10.1007/S10904-023-02901-8/METRICS

Ali, M.A., Saad, H.-E.M., Tighezza, A.M., Khattak, S., Al-Qaisi, S., Faizan, M.: First-principles calculations of novel lead-free X_2GeSnI_6 (X = Rb, Cs) double perovskite compounds for optoelectronic and energy exploitations. J. Inorg. Organom. Polymers Mater. **1**, 1–11 (2023). https://doi.org/10.1007/S10904-023-02901-8

Ali, M.A., Alshgari, R.A., Awadh Bahajjaj, A.A., Sillanpää, M.: The study of new double perovskites K_2AgAsX_6 (X = Cl, Br) for energy-based applications. J. Taibah Univ. Sci. **17**(1), 2170680 (2023d). https://doi.org/10.1080/16583655.2023.2170680

Alnujaim, S., Bouhemadou, A., Chegaar, M., Guechi, A., Bin-Omran, S., Khenata, R., Al-Douri, Y., Yang, W., Lu, H.: Density functional theory screening of some fundamental physical properties of $Cs_2InSbCl_6$ and $Cs_2InBiCl_6$ double perovskites. Eur. Phys. J. B **95**(7), 1–16 (2022). https://doi.org/10.1140/EPJB/S10051-022-00381-2

Ambrosch-Draxl, C., Sofo, J.O.: Linear optical properties of solids within the full-potential linearized augmented planewave method. Comput. Phys. Commun. **175**(1), 1–14 (2006). https://doi.org/10.1016/J.CPC.2006.03.005

Ambrosch-Draxl, C., Majewski, J.A., Vogl, P., Leising, G.: First-principles studies of the structural and optical properties of crystalline poly(para-phenylene). Phys. Rev. B **51**(15), 9668 (1995). https://doi.org/10.1103/PhysRevB.51.9668

Barrows, A.T., Pearson, A.J., Kwak, C.K., Dunbar, A.D.F., Buckley, A.R., Lidzey, D.G.: Efficient planar heterojunction mixed-halide perovskite solar cells deposited via spray-deposition. Energy Environ. Sci. **7**(9), 2944–2950 (2014). https://doi.org/10.1039/C4EE01546K

Behera, D., Kumar Mukherjee, S.: First-principles calculations to investigate structural, optoelectronics and thermoelectric properties of lead free Cs_2GeSnX_6 (X = Cl, Br). Mater. Sci. Eng. B **292**, 116421 (2023). https://doi.org/10.1016/J.MSEB.2023.116421

Bhorde, A., Waykar, R., Rondiya, S.R., Nair, S., Lonkar, G., Funde, A., Dzade, N.Y., Jadkar, S.: Structural, electronic, and optical properties of lead-free halide double perovskite Rb_2AgBiI_6: a combined experimental and density functional theory study. ES Mater. Manuf. **12**, 43–52 (2021). https://doi.org/10.30919/ESMM5F1042

Blaha, P., Schwarz, K., Sorantin, P., Trickey, S.B.: Full-potential, linearized augmented plane wave programs for crystalline systems. Comput. Phys. Commun. **59**(2), 399–415 (1990). https://doi.org/10.1016/0010-4655(90)90187-6

Blaha, P., Schwarz, K., Madsen, G.K.H., Kvasnicka, D., Luitz, J., Laskowsk, R., Tran, F., Marks, L., Marks, L.: WIEN2k: An augmented plane wave plus local orbitals program for calculating crystal properties. Uniw. śląski, (2019)

Blanco, M.A., Francisco, E., Luaña, V.: GIBBS: isothermal-isobaric thermodynamics of solids from energy curves using a quasi-harmonic debye model. Comput. Phys. Commun. **158**(1), 57–72 (2004). https://doi.org/10.1016/J.COMPHY.2003.12.001

Dimitrov, S.D., Durrant, J.R.: Materials design considerations for charge generation in organic solar cells. Chem. Mater. **26**(1), 616–630 (2014). https://doi.org/10.1021/CM402403Z/ASSET/IMAGES/MEDIUM/CM-2013-02403Z_0012.GIF

Fox, M., Bertsch, G.F.: Optical properties of solids. Am. J. Phys. **70**(12), 1269–1270 (2002). https://doi.org/10.1119/1.1691372

Gao, Y., Pan, Y., Zhou, F., Niu, G., Yan, C.: Lead-free halide perovskites: a review of the structure-property relationship and applications in light emitting devices and radiation detectors. J. Mater. Chem. A **9**(20), 11931–11943 (2021). https://doi.org/10.1039/D1TA01737C

Grätzel, M.: The light and shade of perovskite solar cells. Nat. Mater. **13**(9), 838–842 (2014). https://doi.org/10.1038/nmat4065

Husain, M., Rahman, N., Sfina, N., Al-Shaalan, N.H., Alharthi, S., Alharthy, S.A., Amin, M.A., Tirth, V., Khan, R., Sohail, M., Azzouz-Rached, A., Khattak, S.A., Khan, M.Y.: The comparative investigations of structural, optoelectronic, and mechanical properties of $AgBeX_3$ (X = F and Cl) metal halide-perovskites for prospective energy applications utilizing DFT approach. Opt. Quantum Electron. **55**(10), 1–16 (2023). https://doi.org/10.1007/S11082-023-05187-9/FIGURES/9

Islam, M.N., Podder, J., Saha, T., Rani, P.: Semiconductor to metallic transition under induced pressure in $Cs_2AgBiBr_6$ double halide perovskite: a theoretical DFT study for photovoltaic and optoelectronic applications. RSC Adv. **11**(39), 24001–24012 (2021). https://doi.org/10.1039/D1RA03161A

Jamal, M., Bilal, M., Ahmad, I., Jalali-Asadabadi, S.: IRelast package. J. Alloys Compd. **735**, 569–579 (2018). https://doi.org/10.1016/J.JALLCOM.2017.10.139

Jena, A.K., Kulkarni, A., Miyasaka, T.: Halide perovskite photovoltaics: background, status, and future prospects. Chem. Rev. **119**(5), 3036–3103 (2019). https://doi.org/10.1021/ACS.CHEMREV.8B00539/ASSET/IMAGES/MEDIUM/CR-2018-00539A_0060.GIF

Ju, M.G., Chen, M., Zhou, Y., Dai, J., Ma, L., Padture, N.P., Zeng, X.C.: Toward eco-friendly and stable perovskite materials for photovoltaics. Joule **2**(7), 1231–1241 (2018). https://doi.org/10.1016/J.JOULE.2018.04.026

Karki, B.B., Ackland, G.J., Crain, J.: Elastic instabilities in crystals from ab initio stress—strain relations. J. Phys. Condens. Matter **9**(41), 8579 (1997). https://doi.org/10.1088/0953-8984/9/41/005

Khattak, S.A., Wabaidur, S.M., Islam, M.A., Husain, M., Ullah, I., Zulfiqar, S., Rooh, G., Rahman, N., Khan, M.S., Khan, G., Khan, T., Ghlamallah, B.: First-principles structural, elastic and optoelectronics study of sodium niobate and tantalate perovskites. Sci. Rep. **12**(1), 1–12 (2022). https://doi.org/10.1038/s41598-022-26250-7

Khattak, S.A., Abohashrh, M., Ahmad, I., Husain, M., Ullah, I., Zulfiqar, S., Rooh, G., Rahman, N., Khan, G., Khan, T., Salman Khan, M., Shah, S.K., Tirth, V.: Investigation of structural, mechanical, optoelectronic, and thermoelectric properties of $BaXF_3$ (X = Co, Ir) fluoro-perovskites: promising materials for optoelectronic and thermoelectric applications. ACS Omega (2022b). https://doi.org/10.1021/ACSOMEGA.2C05845/ASSET/IMAGES/LARGE/AO2C05845_0011.JPEG

Khattak, S.A., Abohashrh, M., Ahmad, I., Husain, M., Ullah, I., Zulfiqar, S., Rooh, G., Rahman, N., Khan, G., Khan, T., Salman Khan, M., Shah, S.K., Tirth, V.: Investigation of structural, mechanical, optoelectronic, and thermoelectric properties of $BaXF_3$ (X = Co, Ir) fluoro-perovskites: promising materials for optoelectronic and thermoelectric applications. ACS Omega **8**(6), 5274–5284 (2023)

Kiran, S., Mumtaz, U., Mustafa, A., Imran, M., Hussain, F., Rasheed, U., Khalil, R.M.A., Khera, E.A., Nazir, A.: An ab initio investigation of the structural, mechanical, electronic, optical, and thermoelectric characteristics of novel double perovskite halides Cs_2CaSnX_6 (X = Cl, Br, I) for optically influenced RRAM devices. RSC Adv. **13**(16), 11192–11200 (2023). https://doi.org/10.1039/D3RA00078H

Kohn, W., Sham, L.J.: Self-consistent equations including exchange and correlation effects. Phys. Rev. **140**(4A), A1133 (1965). https://doi.org/10.1103/PHYSREV.140.A1133/FIGURE/1/THUMB

Koller, D., Tran, F., Blaha, P.: Improving the modified Becke-Johnson exchange potential. Phys. Rev. B Condens. Matter. Mater. Phys. **85**(15), 155109 (2012)

Landini, E., Reuter, K., Oberhofer, H.: Machine-learning based screening of lead-free halide double perovskites for photovoltaic applications. (2022)

Mir, S.A., Gupta, D.C.: Structural and mechanical stabilities, electronic, magnetic and thermophysical properties of double perovskite Ba_2LaNbO_6: probed by DFT computation. Int. J. Energy Res. **45**(10), 14603–14611 (2021)

Mouhat, F., Coudert, F.X.: Necessary and sufficient elastic stability conditions in various crystal systems. Phys. Rev. B **90**(22), 224104 (2014). https://doi.org/10.1103/PhysRevB.90.224104

Muscarella, L.A., Hutter, E.M.: Halide double-perovskite semiconductors beyond photovoltaics. ACS Energy Lett. **7**(6), 2128–2135 (2022)

Paul, T., Hiralal Makani, N., Sahoo, A., Singh Tanwar, L., Singh, M., Banerjee, R.: Halide perovskites for optoelectronic application. Mater. Today Proc. (2023). https://doi.org/10.1016/J.MATPR.2023.06.327

Poloni, R., Machon, D., Fernandez-Serra, M.V., Le Floch, S., Pascarelli, S., Montagnac, G., Cardon, H., San-Miguel, A.: High-pressure stability of Cs_6 C_{60}. Phys. Rev. B Condens. Matter Mater. Phys. **77**(12), 125413 (2008). https://doi.org/10.1103/PHYSREVB.77.125413/FIGURES/2/MEDIUM

Poloni, R., Fernandez-Serra, M.V., Le Floch, S., De Panfilis, S., Toulemonde, P., Machon, D., Crichton, W., Pascarelli, S., San-Miguel, A.: Pressure-Induced Deformation of the C_{60} Fullerene in Rb_6 C_{60} and Cs_6 C_{60}. Phys. Rev. B Condens. Matter Mater. Phys. **77**(3), 035429 (2008). https://doi.org/10.1103/PHYSREVB.77.035429/FIGURES/10/MEDIUM

Rahman, N., Rauf, A., Husain, M., Sfina, N., Tirth, V., Sohail, M., Khan, R., Azzouz-Rached, A., Murtaza, G., Khan, A.A., Khattak, S.A., Khan, A.: Probing the physical properties of M_2LiCeF_6 (M = Rb and Cs) double perovskite compounds for prospective high-energy applications employing the DFT framework. RSC Adv. **13**(23), 15457–15466 (2023). https://doi.org/10.1039/D3RA01451G

Ren, M., Qian, X., Chen, Y., Wang, T., Zhao, Y.: Potential lead toxicity and leakage issues on lead halide perovskite photovoltaics. J. Hazard. Mater. **426**, 127848 (2022). https://doi.org/10.1016/J.JHAZMAT.2021.127848

Rosales, B.A., Hanrahan, M.P., Boote, B.W., Rossini, A.J., Smith, E.A., Vela, J.: Lead halide perovskites: challenges and opportunities in advanced synthesis and spectroscopy. ACS Energy Lett. **2**(4), 906–914 (2017)

Saddique, J., Husain, M., Rahman, N., Khan, R., Zulfiqar, Iqbal, A., Sohail, M., Khattak, S.A., Khan, S.N., Khan, A.A., Reshak, A.H., Khan, A.: Modeling structural, elastic, electronic and optical properties of ternary cubic barium based fluoroperovskites $MBaF_3$ (M = Ga and In) compounds based on DFT. Mater. Sci. Semicond. Process. **139**(May), 106345 (2022). https://doi.org/10.1016/j.mssp.2021.106345

Saeed, M., Haq, I.U., Saleemi, A.S., Rehman, S.U., Haq, B.U., Chaudhry, A.R., Khan, I.: First-principles prediction of the ground-state crystal structure of double-perovskite halides Cs_2AgCrX_6 (X = Cl, Br, and I). J. Phys. Chem. Solids **160**, 110302 (2022). https://doi.org/10.1016/J.JPCS.2021.110302

Sk, M., Ghosh, S.: 16.35 % efficient $Cs_2GeSnCl_6$ based heterojunction solar cell with hole-blocking SnO_2 layer: DFT and SCAPS-1D simulation. Optik **267**, 169608 (2022). https://doi.org/10.1016/J.IJLEO.2022.169608

Soni, Y., Rani, U., Shukla, A., Joshi, T.K., Verma, A.S.: Transition metal-based halides double Cs_2ZSbX_6 (Z = Ag, Cu, and X = Cl, Br, I) perovskites: a mechanically stable and highly absorptive materials for photovoltaic devices. J. Solid State Chem. **314**, 123420 (2022). https://doi.org/10.1016/J.JSSC.2022.123420

Solid State Physics: Ashcroft, Neil W., Mermin, N. David + Free Shipping. https://www.amazon.com/Solid-State-Physics-Neil-Ashcroft/dp/0030839939 (Accessed 2022–11–16)

Tang, T., Tang, Y.: First principle comparative study of transitional elements Co, Rh, Ir(III)-based double halide perovskites. Mater. Today Commun. **34**, 105431 (2023). https://doi.org/10.1016/J.MTCOMM.2023.105431

Thawarkar, S., Rondiya, S.R., Dzade, N.Y., Khupse, N., Jadkar, S.: Experimental and theoretical investigation of the structural and opto-electronic properties of Fe-doped lead-free $Cs_2AgBiCl_6$ double perovskite. Chem. A Eur. J. **27**(26), 7408–7417 (2021). https://doi.org/10.1002/CHEM.202004902

Tyuterev, V.G., Vast, N.: Murnaghan's equation of state for the electronic ground state energy. Comput. Mater. Sci. **38**(2), 350–353 (2006). https://doi.org/10.1016/J.COMMATSCI.2005.08.012

Vijayakumar, M., Gopinathan, M.S.: Spin-orbit coupling constants of transition metal atoms and ions in density functional theory. J. Mol. Struct. Theochem. **361**(1–3), 15–19 (1996). https://doi.org/10.1016/0166-1280(95)04297-0

Xing, G., Mathews, N., Sun, S., Lim, S.S., Lam, Y.M., Graẗzel, M., Mhaisalkar, S., Sum, T.C.: Long-range balanced electron-and hole-transport lengths in organic-inorganic $CH_3NH_3PbI_3$. Science **342**(6156), 344–347 (2013). https://doi.org/10.1126/SCIENCE.1243167/SUPPL_FILE/XING.SM.PDF

Authors and Affiliations

Shaukat Ali Khattak[1] · Saikh Mohammad Wabaidur[2] · Asma A. Alothman[2] · Mudasser Husain[3] · Malak Azmat Ali[4] · Nasir Rahman[5] · Irfan Ullah[1] · Syed Zulfiqar[1] · Gul Rooh[1] · Tahirzeb Khan[1] · Gulzar Khan[1]

✉ Shaukat Ali Khattak
shaukat.khattak@awkum.edu.pk

[1] Department of Physics, Abdul Wali Khan University, Mardan 23200, Pakistan

[2] Chemistry Department, College of Science, King Saud University, 11451 Riyadh, Saudi Arabia

[3] Institute of Condensed Matter and Material Physics Department of Physics, Peking University, Beijing 100871, People's Republic of China

[4] Department of Physics, Government Post Graduate Jahanzeb College Saidu Sharif, Swat 19130, Khyber Pakhtunkhwa, Pakistan

[5] Department of Physics, University of Lakki Marwat, Lakki Marwat 28420, Pakistan